Analysis of the different regimes of atmospheric turbulence observed during a single night

S. Viana[1](*), E. Terradellas[1](**), C. Yagüe[2](***) and G. Maqueda[3](✱✱)

[1] *Agencia Estatal de Meteorología - Barcelona, Spain*

[2] *Departamento de Geofísica y Meteorología, Universidad Complutense de Madrid Madrid, Spain*

[3] *Departamento de Astrofísica y CC. de la Atmósfera, Universidad Complutense de Madrid Madrid, Spain*

Summary. — This work presents a comprehensive study of the different turbulence regimes observed during a night (27-28 June 2006) at the CIBA (Research Centre for the Lower Atmosphere), located in the northern part of the Iberian Peninsula, in the Duero valley, over relatively flat and homogeneous terrain. The synoptic situation was dominated by an Atlantic anticyclone, with a weak northern flow over the area of interest. Nevertheless, the actual meteorological evolution was mainly driven by the mesoscale conditions. The meteorological sequence of events were the irruption of a drainage flow, part of a nocturnal circulation established over the whole basin, and finally, the onset of a thick and dense fog layer that covered the region during several hours. These facts produced sudden changes both in the turbulence regime and in the stability of the lowest layers of the atmosphere, so that, three periods, with moderately stable, weakly stable and neutral stratification can be perfectly distinguished. The study includes the analysis of different observational datasets, gathered during SABLES-2006, a field campaign especially designed to improve the knowledge on the nocturnal boundary layer.

PACS `92.60.Fm` – Boundary layer structure and processes.
PACS `92.60.hk` – Convection, turbulence, and diffusion.

(*) E-mail: `sviana@inm.es`
(**) E-mail: `enric@inm.es`
(***) E-mail: `carlos@fis.ucm.es`
(✱✱) E-mail: `gmaqueda@fis.ucm.es`

1. – Introduction

The Atmospheric Boundary Layer (ABL) is the part of the troposphere directly influenced by the Earth's surface. The Stable Atmospheric Boundary Layer (SBL) is formed when the surface is cooler than the overlying air [1]. It often occurs at night over land, and then, this layer is also known as Nocturnal Boundary Layer (NBL), the framework of the current study. Among the phenomena that take place in the NBL, radiative flux divergence, intermittent and patchy turbulence, slope flows, low-level jets (LLJs), elevated turbulence, shear instabilities, wave generation and breaking, wave-turbulence interactions or fog formation may be highlighted. In recent years, much effort has been paid to the understanding of the physical processes related to the SBL. Realistic parameterizations of the SBL are needed in order to achieve a proper representation of the ABL in Numerical Weather Prediction (NWP) models. On the experimental side, several field campaigns have taken place, both in mid-latitudes [2-5] and at polar sites [6, 7]. Along the night, the relative importance between the mechanical generation of turbulence and the damping produced by stability can change quite quickly, leading to different levels of turbulent mixing, which sometimes is intermittent or sporadic. One of the less known issues in the SBL studies is the interaction between turbulence and waves: as stability increases, vertical turbulent motions are suppressed, but buoyant oscillations—internal gravity waves—may appear. Then, turbulence can be suppressed or enhanced by the passage of gravity waves, can ride up and down hundreds of meters on these waves, and thus nonlinear interaction is fundamental [8].

Another important object of study is the fog formation and its relation to turbulence. There are several important effects of fog on human activities, especially in the field of transportation. The impact of fog on ground, water and air transport is, respectively, discussed in [9-11]. Nevertheless, the production of precise fog forecasts still constitutes an unsolved issue for operational weather services. The physical processes involved in its evolution are not yet completely understood and, therefore, not accurately enough parameterised in NWP models [12, 13]. In particular, the role of turbulence in the evolution of radiation fog remains as one of the most controversial points. Whereas several authors, such as Roach *et al.* [14] state that turbulence is a factor that inhibits the onset of radiation fog, others (*e.g.* [15]) support the theory that turbulence constitutes a contributing factor. A combination of both theories leads to the conclusion that there is a threshold relationship between turbulence and fog formation [16]. It is interesting to analyse the vertical profiles of the different meteorological magnitudes during fog episodes. These profiles and, therefore, the value and even the sign of the turbulent fluxes, can notably change along the different stages of the fog evolution. In the first stages of the evolution of radiation fog, before sunrise, when there are no significant radiative fluxes near the surface, if the ground heat flux is not very large, sensible and latent fluxes tend to cancel each other, a situation that is not common in a clear NBL [17]. In these situations, while there is still a downward sensible heat flux, the latent heat flux may point upwards, the evaporation of ground water feeding the fog growth.

In the current work, a night from the SABLES-2006 (Stable Atmospheric Boundary Layer Experiment in Spain) field campaign [4] is analysed (June 27-28). During this night, several of the above described features related with the NBL may be observed and analysed: stable stratification, katabatic winds, LLJs and fog formation. Section **2** describes the site where the experiment took place and the instrumentation deployed. Section **3** explains the methods used to analyse the time series of observational data: MultiResolution Flux Decomposition and Wavelet Transform. The evolution of the

TABLE I. – *Main instruments installed on the* 100 m *mast.*

Instrument	Altitude (m)	Sampling rate (Hz)
Metek USA-1 Sonic anemometers	3-19.6-96.6	20
Wind vanes	9.6-34.6-74.6-98.6	5
Cup anemometers	2.3-9.6-34.6-50-74.6-98.6	5
Platinum resistance thermometers	2.3-10.5-20.5-35.5-97.5	1
Relative humidity sensors	10-97	1
Microbarometers	20-50-100	2

meteorological conditions and the turbulence regimes observed along the night is described in sect. **4**. Finally, the conclusions are stated in sect. **5**.

2. – Site and instrumentation

This work is based on observational data from the Research Centre for the Lower Atmosphere (CIBA in Spanish). This atmospheric laboratory is located at $41°49'$N, $4°56'$W, 840 m above sea level, about 30 km NW from Valladolid city, in the Northern Spanish Plateau, on relatively flat and homogeneous terrain. It has to be noticed that GMT matches the local standard time. The measurements were collected during the SABLES-2006 field campaign, which took place along June and July 2006. The campaign was designed to fill in some gaps detected during previous campaigns carried out at the same place, especially regarding the observation of internal gravity waves [2]. The records that have been used come from the following sets of instruments:

– Permanent instrumentation of the laboratory, installed on a 100 m mast. It consists of fast-response sonic anemometers and a set of conventional sensors that measure wind speed and direction, temperature and relative humidity at different heights, soil temperature and atmospheric pressure at surface (see table I for details). This instrumentation was installed by the National Risoe Laboratory in 2001, as part of a project to upgrade the 100 m tower, which had been active since the 1980s [18,5]. In addition, a RASS-SODAR profiler operates continuously providing wind and temperature data up to 500 m above ground level (AGL).

– Six Paroscientific microbarometers (three of them installed at 20, 50 and 100 m AGL on the tower, and the other three deployed at 1 m AGL on a triangular array of approximately 200 m side). These devices were configured to measure the absolute pressure at a sampling rate of 2 Hz and a resolution around 0.002 hPa. These values have been set in a compromise between the temporal resolution and the necessary accuracy to register low-amplitude pressure perturbations. The records of these microbarometers are ideal for observing the propagation of wave-like structures and for estimating the wave parameters (see [19]).

– A tethered balloon that was operated during nighttime, when wind conditions were favorable. Five vertical soundings were completed during the night under study, three of them exceeding a height of 800 m AGL.

3. – Methodology

Different turbulence and stability parameters are evaluated along the night in order to determine the main characteristics of the NBL. These parameters will be related to several mesoscale phenomena observed during the night, such as the irruption of a drainage flow, the presence of a LLJ or the development of a fog layer. They are listed and defined in Appendix A. The stability parameters (gradient Richardson number and inversion strength) are evaluated from five-minute averages of tower data. On the other hand, the turbulent parameters are estimated with fast data (20 Hz) from the sonic anemometers using the Wavelet Transform (WT) or the MultiResolution Flux Decomposition (MRFD), two very useful tools to apply in the analysis of a non-stationary boundary layer, as it usually is the SBL.

3˙1. *MultiResolution Flux Decomposition*. – Turbulent fluxes have been traditionally evaluated through eddy covariances, which are calculated over a previously defined averaging length that is fixed for the whole dataset [1]. For an accurate evaluation of the turbulent fluxes and other derived parameters, the chosen averaging length must be able to properly capture the effects of the turbulent fluctuations, while preventing the inclusion of larger-scale contributions. The averaging length must be ideally close to a minimum of energy in the spectrum of the turbulence, the so-called gap, which separates turbulent eddies from larger-scale motions, such as mesoscale flows or wavy structures. An *a priori* definition of the averaging length is possible under neutral or unstable conditions, when the flow is often stationary and the time scale of the spectral gap is roughly constant. However, turbulence developed in stably-stratified flows is much more complex: turbulent fluxes are small, oscillations are typically non-stationary, the position of the gap is variable and sometimes it is difficult or even impossible to define a suitable averaging length, because turbulent and larger-scale motions completely overlap. The MRFD [20, 21] is an alternative approach to evaluate variances and covariances, which reduces errors caused by the contamination of turbulent fluxes by large-scale structures. The variance of a time series can be calculated from the integration of its power spectrum. Similarly, the covariance of two time series results from the integration of the corresponding cospectrum [1]. The MRFD method can derive the spectrum of a time series, not through the Fourier transform, but using an iterative process in which, at every step, the time series with 2^n points and sampling period ΔT is recursively filtered by subtracting non-overlapping moving averages of decreasing length 2^i ($i = n, n-1, \ldots, 1$). The resulting time series retain only fluctuations up to the timescale corresponding to the length of the moving average (*i.e.* $2^i \Delta T$). In every step, the variance is calculated. The differences between consecutive variances form the spectrum of the time series, so that these coefficients represent the contribution to the variance from structures of different timescales. In the same way, when applied to two time series of different variables (*i.e.* vertical wind speed w and temperature T), the resulting multiresolution coefficients (the differences between consecutive covariances) represent the contributions to the total flux from structures of different timescales. The convenience of computing spectra and cospectra using MRFD instead of Fourier Transform in turbulence studies has been discussed in detail in [21-23]. One of the main advantages is that this method does not rely on the periodicity of the time series (strictly speaking, turbulent motions are not periodic events as noted by Tennekes [24]). Instead, the signal is decomposed locally, so that the peak in spectra and cospectra depends only on the mean timescale of the local—in a temporal sense—turbulent events. In contrast, the peak in Fourier power
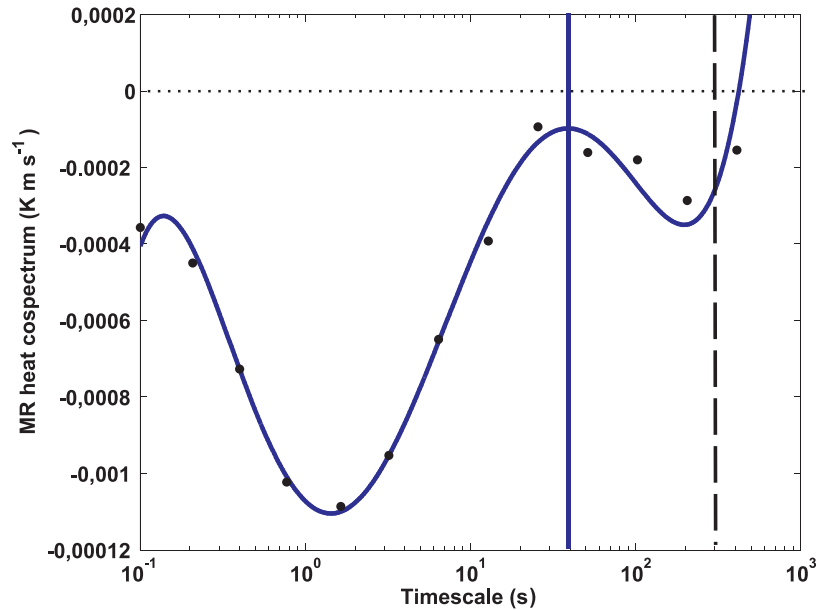
Fig. 1. – Example of a typical MRFD heat cospectrum under stable stratification, and the polynomial fit used to define the gap. Solid and dashed vertical lines mark the timescale of the found gap and the typical 5 min averaging length used in the eddy covariance method.

spectra depends on the principal periodicity present in the whole time series. Furthermore, in turbulence studies the spacing between local events might itself constitute a relevant periodicity of the time series, making ambiguous the interpretation of the peak in the Fourier cospectra [21]. For similar reasons, the location of the turbulent gap is better determined using MRFD.

The vertical heat fluxes for the whole night have been estimated using 13.6-minute subseries (820 seconds, 2^{14} data points) of vertical velocity and potential temperature collected by the sonic anemometers set at 3 and 19.6 m AGL. An algorithm similar to that used by Voronovich and Kiely [23] has been implemented to define the gap in the cospectra: every single MRFD heat cospectrum is fitted to a 5th-order polynomial, and then the timescale of the spectral gap is estimated according to a criterion based on the first occurrence of a zero crossing, an inflexion point or a minimum of the absolute value in the fitted cospectrum after the turbulent peak of maximum downward (negative) or upward (positive) heat flux. An example of a MRFD heat cospectrum under stable stratification is shown in fig. 1. The x-axis has been plotted with a logarithmic scale, since the timescales of the motions resolved by the sonic anemometers cover several orders of magnitude, ranging from 10^{-1} to 10^2 s. The coefficients of the cospectra define a negative—downward—turbulent flux, as expected under stable conditions. The solid vertical line marks the timescale of the gap found by the algorithm (≈ 40 s), and a dashed vertical line is placed at a timescale of 5 minutes, the typical averaging length from the eddy covariance method. The error induced by the use of the eddy covariance method is represented by the fraction of the cospectrum between both timescales (in this example, it would lead to overestimation of the negative heat flux). The turbulent

fluxes and variances are finally computed through the integration of the multiresolution spectra and cospectra up to the timescale of the gap found by the algorithm described above. This algorithm sometimes fails to find a gap in the cospectra of vertical heat flux at 19.6 m AGL. The cospectrum of some subseries shows an erratic shape and no clear gap can be defined. In these cases, the turbulent fluxes and other derived parameters are not evaluated and blanks will appear in the corresponding plots. For the same reason, the method has not been applied to data recorded at 96.6 m AGL. At that height, the vertical fluxes are very small during most part of the night, the cospectra are often quite plain for the turbulent timescales, and estimations of the gap are not reliable.

$3^\cdot 2$. *Wavelet Transform.* – The Wavelet Transform (WT) [25] is a mathematical tool that enables the analysis of non-stationary time series. It gives a time-frequency representation of them providing time and frequency information simultaneously. The WT of a time series f at the scale s and time t, here represented F_{st}, is the convolution of the series with a dilated and translated wavelet (Ψ_{st}). That is

$$(1) \qquad\qquad F_{st} = \int_{-\infty}^{\infty} f(t')\Psi_{st}^*(t')\mathrm{d}t',$$

where (*) denotes complex conjugation. A general principle of the theory is that the WT fulfils energy conservation for the whole series [26]. If the series is real and the wavelet is an analytic function:

$$(2) \qquad\qquad \int_{-\infty}^{\infty} \mathrm{d}t\,(f(t))^2 = \frac{2}{C_\psi} \int_0^{\infty} \int_{-\infty}^{\infty} \frac{\|F_{st_0}\|^2}{s^2}\mathrm{d}s\mathrm{d}t_0,$$

where C_Ψ is a normalizing factor, which depends on the mother wavelet:

$$(3) \qquad\qquad C_\Psi = \int_{-\infty}^{\infty} \frac{\mathrm{d}\zeta}{\zeta}\overline{|\Psi(\zeta)|}^2,$$

$\overline{\Psi(\zeta)}$ being the Fourier transform of the wavelet.

During recent years, an approach based on the Wavelet Transform (WT) has been developed to estimate the Turbulent Kinetic Energy (TKE) and the turbulent fluxes in the SBL [27-29]. The authors define a TKE-density per scale unit as

$$(4) \qquad\qquad \mathrm{TKE}_{st} = \frac{1}{C_\Psi}\frac{\|U_{st}\|^2}{s^2} + \frac{1}{C_\Psi}\frac{\|V_{st}\|^2}{s^2} + \frac{1}{C_\Psi}\frac{\|W_{st}\|^2}{s^2},$$

where U_{st}, V_{st} and W_{st} are the wavelet transforms of the time series of the wind components (u, v, w) at the scale s and time t. In a similar way, the vertical heat flux per scale unit at the scale s and time t is

$$(5) \qquad\qquad H_{st} = \rho\,c_p\frac{2}{C_\Psi}\frac{\Theta_{st}W_{st}^*}{s^2},$$

where ρ is the air density, c_p is the specific heat at constant pressure and Θ_{st} is the wavelet transform of the time series of potential temperature. In the present study, the chosen wavelet is the Morlet function, a plane wave modulated by a Gaussian. This
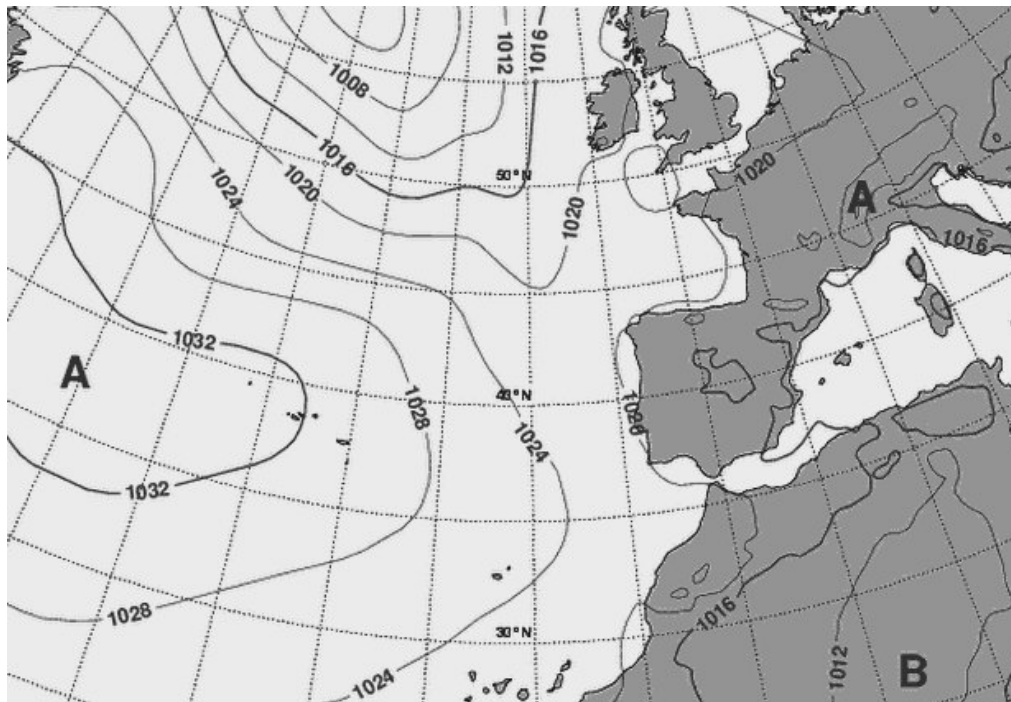
Fig. 2. – Surface analysis of 28 June 2006 at 0000 GMT made by the HIRLAM-0.5 model.

mother function has a well-defined relationship between scales (s) and equivalent Fourier periods, and has been widely used for the analysis of geophysical time series [30]. Its sinusoidal shape is suitable for studies in the stable boundary layer, where wavy motions are frequent.

The method yields a time-frequency map of the turbulent magnitudes. That is, it provides information on the contribution of the different spectral ranges to the total TKE or fluxes. It needs, as the eddy covariance method does, an *a priori* definition of the spectral boundary of the turbulence. Nevertheless, as shown by Cuxart *et al.* [28], the effectiveness of the Morlet wavelet transform as a filter is higher compared to the averaging method (see in [28], fig. 1, the transfer functions of WT and Reynold's filters). Thus the existence of a spectral gap to prevent the contamination of the turbulent estimates by large scale motions is not strictly necessary in the WT method. In this work, wavelet estimates of turbulent parameters have been made through the integration of spectral contributions up to a period of 5 minutes.

4. – Results

The synoptic-scale analysis of the sea-level pressure at 0000 GMT on 28 June 2006 made by the HIRLAM-0.5 model [31] presents a weak horizontal pressure gradient over the Iberian Peninsula (fig. 2). This situation represents the ideal framework for the establishment of a stably-stratified nocturnal atmospheric boundary layer with weak wind and a strong radiative cooling. Nevertheless, the moderate winds recorded during most part of the night cause a higher production of mechanical turbulence, enhance the vertical mixing and, therefore, reduce the close-to-ground cooling rate.
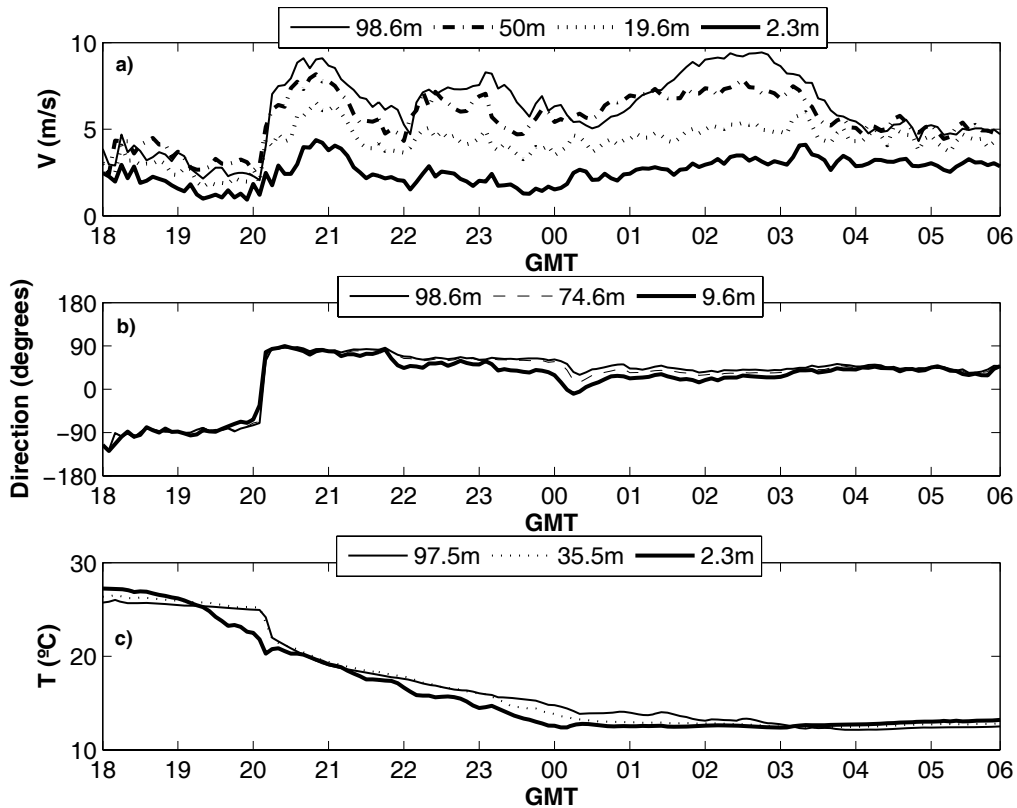
Fig. 3. – Evolution of a) wind speed at 2.3, 19.6, 50 and 98.6 m AGL, b) wind direction at 9.6, 74.6 and 98.6 m AGL and c) temperature at 2.3, 35.5 and 97.5 m AGL.

The reason of this situation lies in the fact that the main characteristics of the boundary layer observed at the CIBA throughout the night 27-28 June are determined by the mesoscale circulation established within the Duero basin. This circulation is the consequence of the organization at the scale of the basin of different topographically induced winds, with the presence of slope and out-valley circulations and the possible formation of cold pools. The importance of this mesoscale activity becomes evident with the outbreak of a katabatic flow around 2010 GMT and the formation of fog around 0310 GMT. These milestones represent sudden changes in the turbulence regime of the lowest atmospheric layers.

4˙1. *Evolution of the structure of the NBL along the night 27-28 June 2006.* – The transition from the daytime convective conditions to the nocturnal stable regime of the boundary layer takes place in a similar way as many other nights of the SABLES-06 campaign [4]. During the late evening and first night hours (1800-2000 GMT), the diurnal westerly flow slowly weakens to a minimum (fig. 3a), with little wind shear and significant surface cooling (figs. 3a and 3c). Scattered stratocumulus with the base above 1000 m AGL, coming from the convective clouds developed during the previous afternoon, are observed. The stratification quickly increases, with the Richardson number well above the critical value (fig. 4a), and the turbulent oscillations nearly suppressed (fig. 4c).
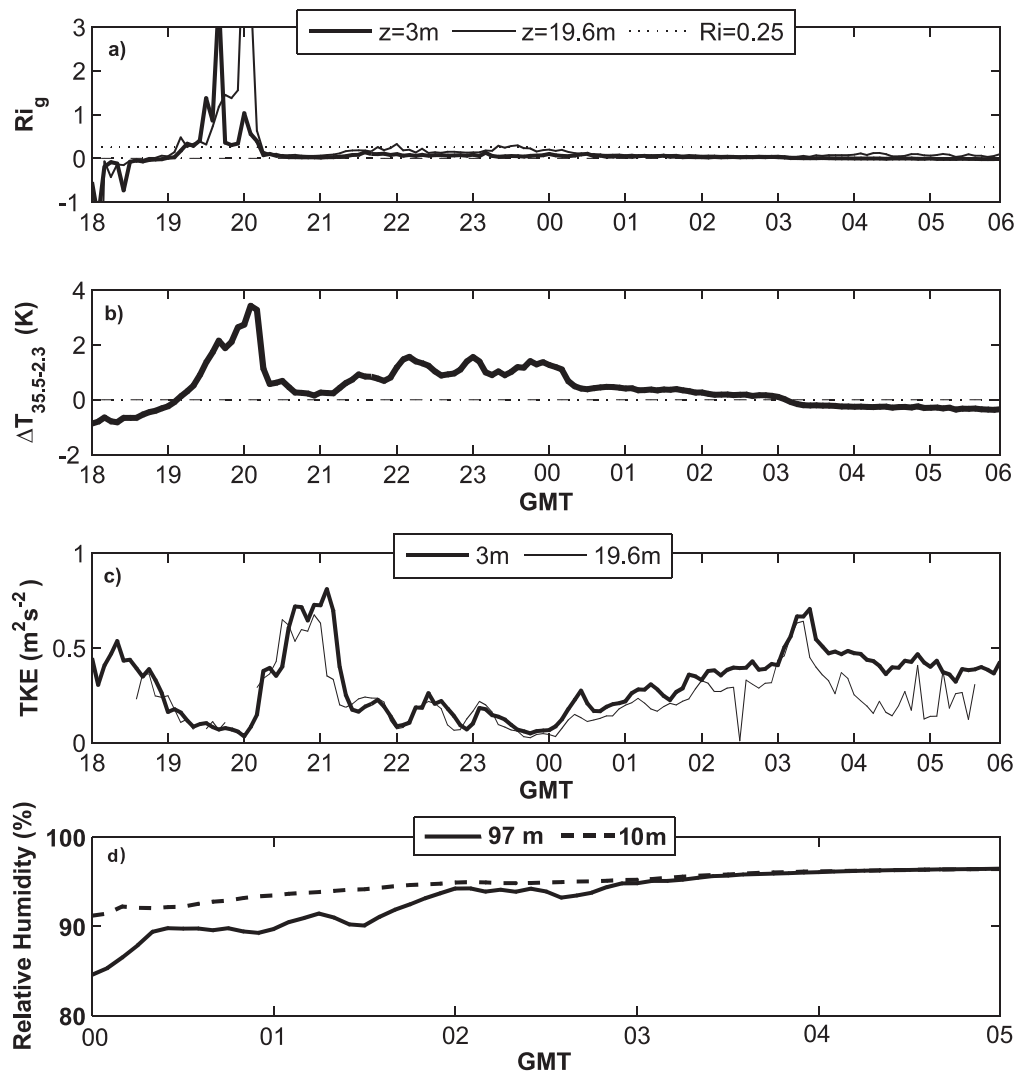
Fig. 4. – Evolution of a) gradient Richardson number at 3 and 19.6 m AGL, b) inversion strength between 35.5 and 2.3 m AGL, c) Turbulent Kinetic Energy at 3 and 19.6 m AGL and d) relative humidity at 10 and 97 m AGL.

This situation is suddenly interrupted by the irruption of an easterly drainage flow around 2010 GMT. A cool air mass of several tens of meters deep arrives from more elevated regions. It is a fact that occurs very often at the CIBA during clear and low windy nights, as part of a mesoscale circulation that is established in the whole Duero valley (see [5]). The sudden decrease of temperature (increase of density) can be clearly noticed in fig. 5, which represents the evolution of the atmospheric pressure in the layer between 20 and 50 m AGL.

Nearly the whole night, from the irruption of the katabatic flow onwards, there is an elevated thermal inversion that separates the cool air mass flowing from more elevated
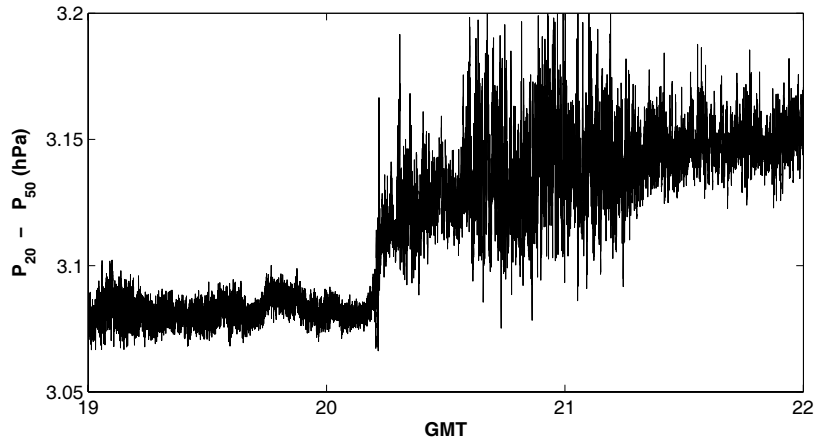
Fig. 5. – Difference between the records of two microbarographs set at 50 and 20 m AGL (in hPa) between 1900 and 2200 GMT on 27 June 2006.

regions and the warmer mass overlying it. Nevertheless, during the first hour, the turbulence is too strong to keep a neat boundary between both air masses. At this time, the main features of the NBL are a strong wind shear and an eroded thermal inversion (fig. 4b), that becomes weak and shallow. The stratification gets close to neutral conditions; the strong vertical mixing prevents the formation of a low-level jet, and the records show moderate northeast winds, with speeds ranging from 2-3 m s^{-1} at low levels to 7-9 m s^{-1} at the upper levels of the mast. As the strength of the turbulence declines, the column progressively stabilizes, and well before midnight, the cloudiness completely disappears. A clear inversion appears in the separation between both superposed air masses and a LLJ develops at this boundary. At 0100 GMT, a peak in the wind profile is clearly visible at 60-80 m AGL in the SODAR record (fig. 6). The inversion progressively strengthens, but it keeps a relatively steady height, about 100 m AGL. The height of the LLJ is roughly the same, its peak exceeding 10 m s^{-1} around 0300 GMT according to SODAR data. Similar conclusions can be drawn from hourly soundings (not shown).

The onset of fog dramatically alters the stability of the column. The breaking point is produced around 0310 GMT, when the ground inversion breaks up (fig. 4b), the vertical thermal profile becomes nearly neutral, and the relative humidity at 97 m equals the value registered at 10 m (fig. 4d): the layer is virtually saturated. The stronger mixing within the fog layer reduces the vertical wind shear: the different levels of the mast show now a northeast wind between 3 and 5 m s^{-1} (fig. 3a).

This fog layer progressively deepens. First, the fog fills the complete depth of the lower mass and then, it pushes the inversion upwards. The SODAR records (figs. 6 and 7) clearly show the thermal inversion above the fog layer and the LLJ well above 200 m at 0500 GMT. The temperature at the lower levels tends to grow, because elevated warmer layers are progressively incorporated into the mixed air mass. This increase of temperature requires an important water inflow into the fog layer in order to keep the air saturated. The water comes from surface evaporation, a mechanism that has already been described by Terradellas et al. [17] for other fog events. The surface evaporation implies an upward latent heat flux. This flux is mainly balanced by an upward soil heat flux that is considerably large because the soil temperature at a 5 cm depth is 20 °C,
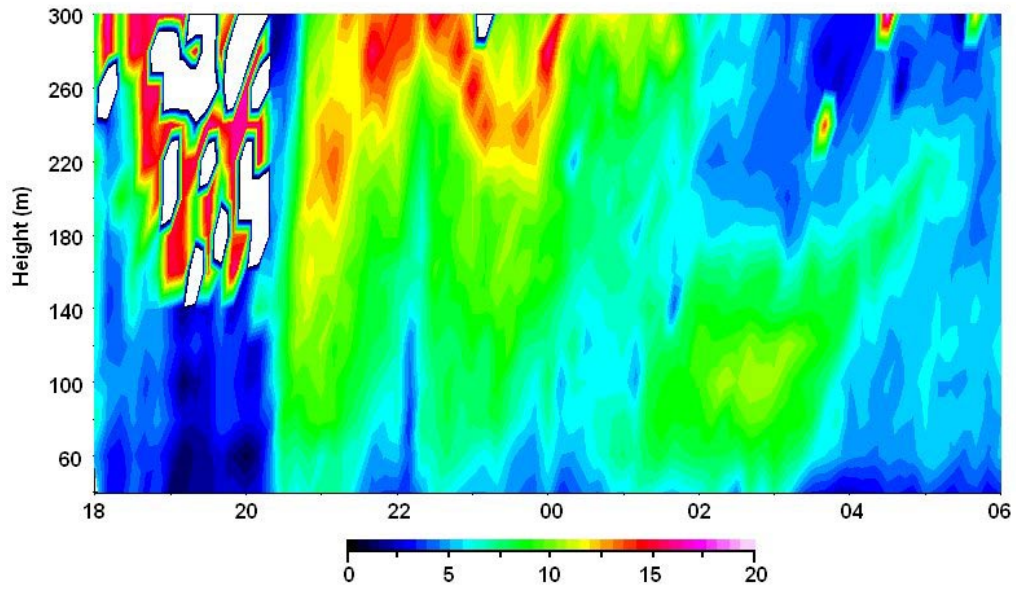
Fig. 6. – Evolution of the wind speed (in m s^{-1}) estimated by the SODAR during the night 27-28 June 2006.
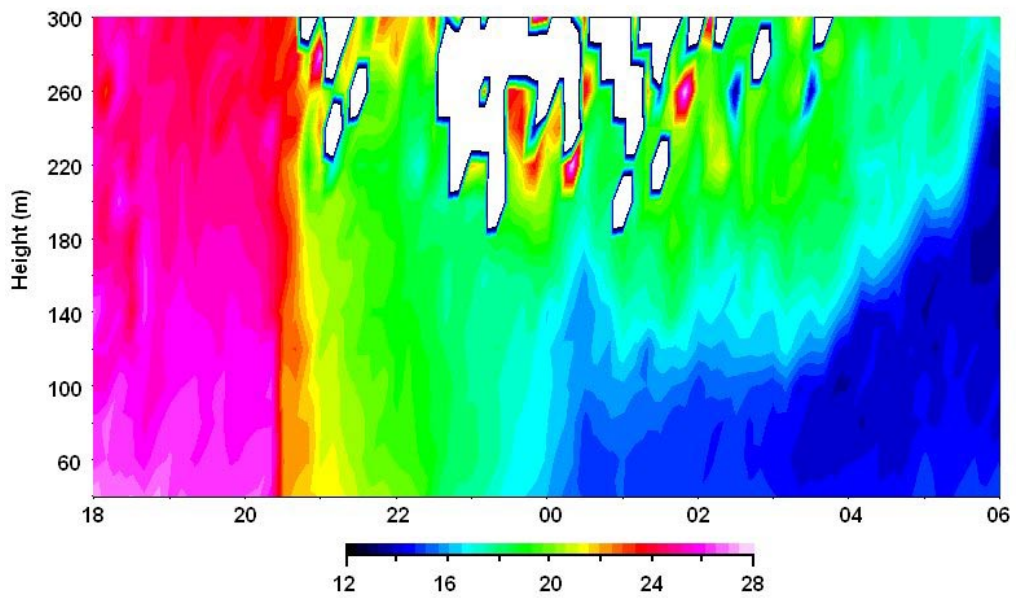

Fig. 7. – Evolution of the air temperature (in Celsius) estimated by the SODAR during the night 27-28 June 2006.
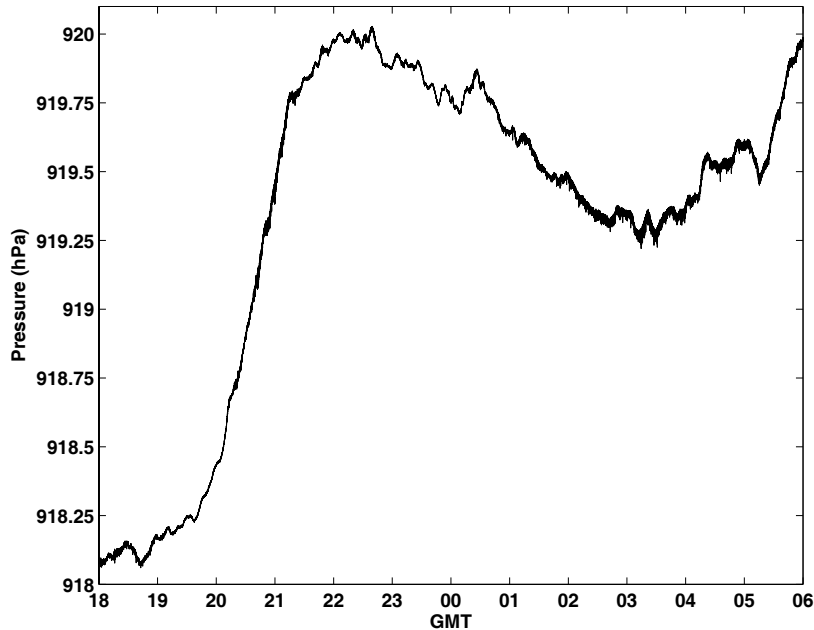
Fig. 8. – Evolution of the surface pressure recorded by one of the microbarographs of the array. The oscillations from 2100 GMT onwards are clearly visible.

about 8 °C higher than the surface air temperature. The other terms of the energy budget are small during the first stages of the fog evolution. The thickness of the fog layer reaches nearly 250 m at 0600 GMT. From that time, the fog evolves to stratus. Both the base and the top of the stratus progressively rise until 1000 GMT, when the sky becomes completely clear.

Vertical motions of diverse origins displace air parcels up or down. When it happens close to the inversion level, it results in undulations of the air mass separation, which cause oscillations in the atmospheric pressure measured below (internal gravity waves). The presence of waves is clearly visible in the pressure records after 2000 GMT (fig. 8). Some characteristics of these waves may be represented using the wavelet transform. Figure 9 shows the energy density per period unit of the time series of atmospheric pressure measured by one of the microbarographs of the array. There is strong activity for periods over 5 minutes.

4˙2. *The evolution of the turbulence regime*. – The MRFD method, described in subsect. **3**˙1, has been applied to data gathered by sonic anemometers set at 3 and 19.6 m AGL. Figure 10 shows the variation of the gap along the night. The spectral contributions to the turbulent parameters (variances and covariances of wind speed components and temperature) have been integrated up to the timescale of the spectral gap found in every vertical heat flux cospectrum. Figure 11 shows the evolution of friction velocity, temperature variance and vertical heat flux along the night at 3 and 19.6 m AGL. In turn, the WT method, described in subsect. **3**˙2, has been applied to estimate the TKE and the vertical heat flux at 19.6 and 96.6 m (fig. 13). In this case, the spectral contributions have been integrated up to a 5-minute period. Therefore both MRFD and WT have been
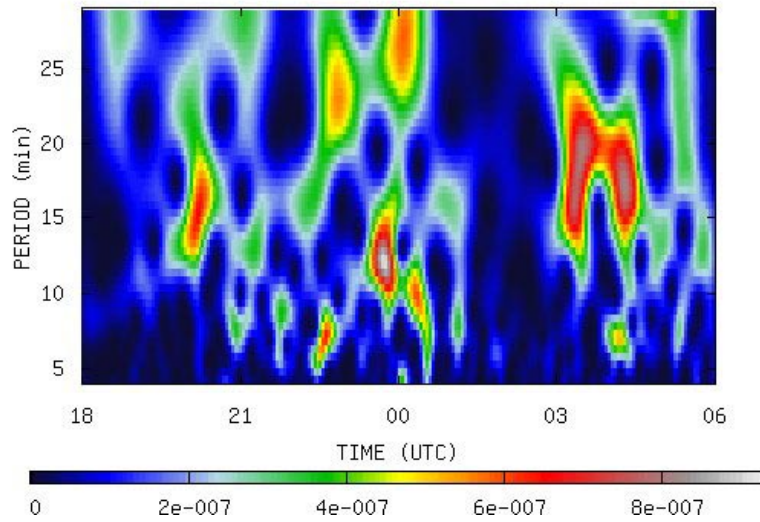
Fig. 9. – Wavelet energy density per unit period ($hPa^2\,s^{-1}$) of the time series of surface pressure recorded by one of the microbarographs of the array. The wave activity between 2100 and 0500 GMT is clearly visible, with periods between 5 and 30 minutes.
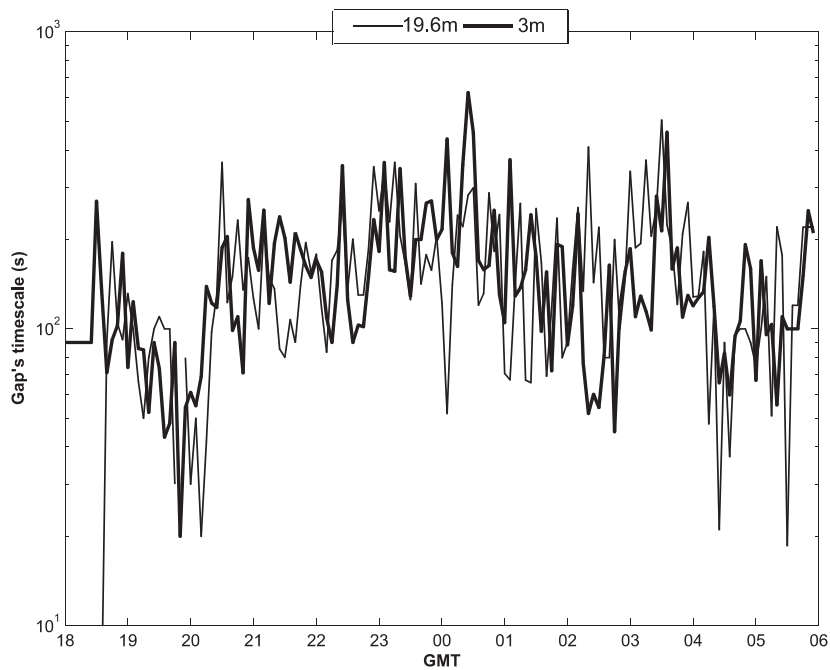

Fig. 10. – Evolution of the spectral gap that is used as the upper integration timescale in the MRFD calculations at 3 at 19.6 m AGL.
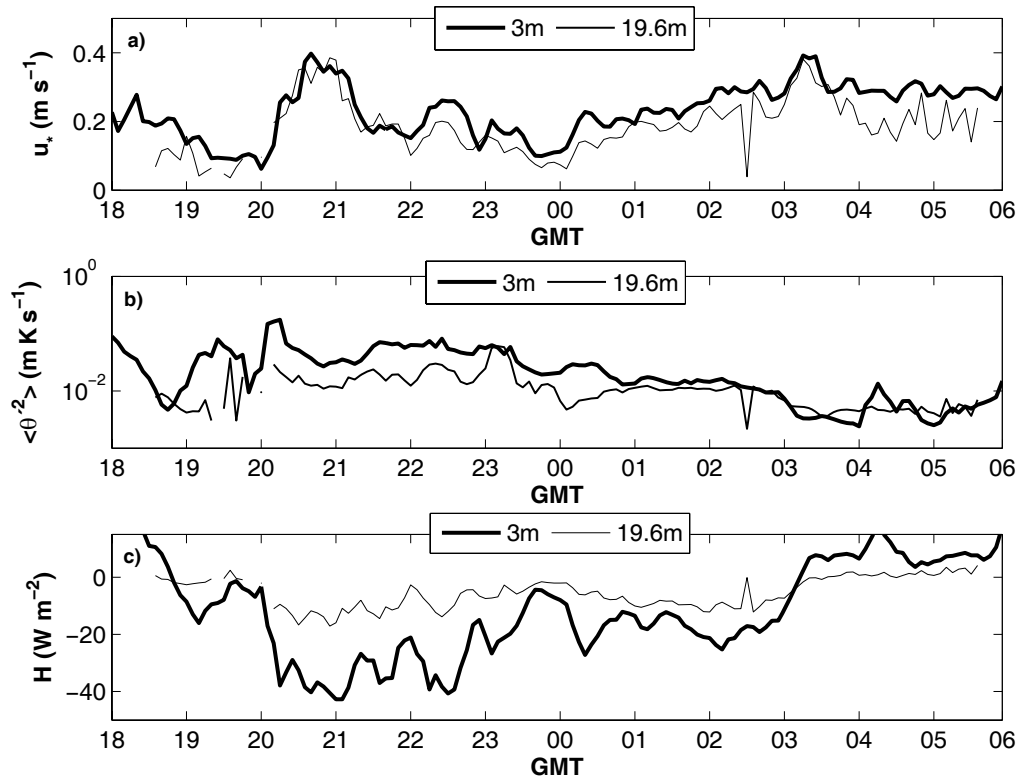
Fig. 11. – Evolution at 3 and 19.6 m AGL of a) friction velocity, b) temperature variance and c) vertical heat flux.

applied at the intermediate sonic level ($z = 19.6$ m), as a consistency check between the two methods.

During the late evening and first part of the night, before the outbreak of the drainage flow, the spectral characteristics of the turbulence change in response to the strengthening of the ground thermal inversion (fig. 4b). During this period, the negative buoyancy developed due to the increasing stability (fig. 4a) inhibits vertical motions. The turbulent peaks in the heat flux cospectra, which is proportional to the temporal and spacial scale characterizing the mean turbulent eddies [22, 23], take values smaller than during subsequent hours (when the drainage flow lowers the stability). As a result, the cospectra during these early hours of the night are more plate-shaped (platykurtic), highlighting a more homogeneous distribution of the turbulent eddies along the different timescales (not shown). The gap progressively shifts from 1-2 minutes to lower timescales, well below one minute (fig. 10). This suggests a negative dependence of the gap's timescale with the stability, in agreement with results from other studies [23]. The turbulence is strongly inhibited: the plots of TKE (figs. 4c and 13a) show very small values at all levels. In spite of the weakness of vertical motions, the temperature variance close to the ground (fig. 11b) is still high, as a consequence of the strong vertical gradient of temperature. Nevertheless, the eddy exchange coefficients, both for heat and momentum (fig. 12) and, consequently, the vertical heat flux (figs. 11c and 13b) and the friction
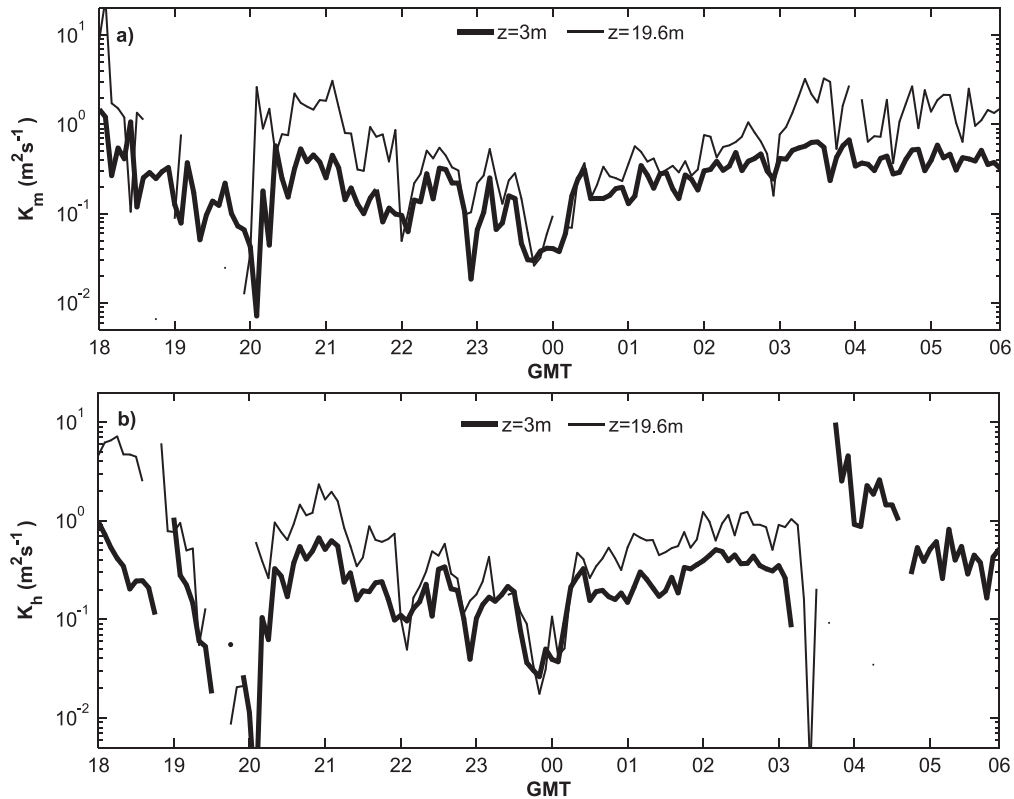
Fig. 12. – Evolution of the eddy exchange coefficients at 3 and 19.6 m AGL for a) momentum (K_m) and b) heat (K_h). Negative (counter-gradient) values are not shown in these plots.

velocity (fig. 11a) are very small. It may be noticed that the vertical heat flux at 96.6 m AGL is still positive.

The outbreak of the katabatic flow entails a sudden increase in the turbulence. The turbulent kinetic energy reaches its highest values along the night, slowly decreasing from surface upwards. Meanwhile, the stability decreases, the gradient Richardson number and the inversion strength becoming close to zero. The heat flux cospectra show well-defined peaks around 2-5 s approximately (not shown): the size (or timescale) distribution of the turbulent eddies is less homogeneous. The decreasing stability also affects the location of the gap, which is now found around 2-3 minutes. The strong turbulence implies high eddy exchange coefficients (fig. 12). The friction velocity is also large because, besides the high exchange coefficients, there is a considerable vertical wind shear. On the other hand, the negative vertical heat flux rapidly decays with height, because of the scarce thermal gradient, resulting in a considerable heat flux divergence that contributes to cooling the air close to the surface (fig. 11c).

From 2100 to 2400 GMT, there is a progressive decrease in the turbulence levels with an increasing stability and a strengthening ground inversion. The eddy exchange coefficients go down, in parallel with the energy of the turbulence, and so do the friction velocity and the vertical heat fluxes, which become very close to zero. Since the heat
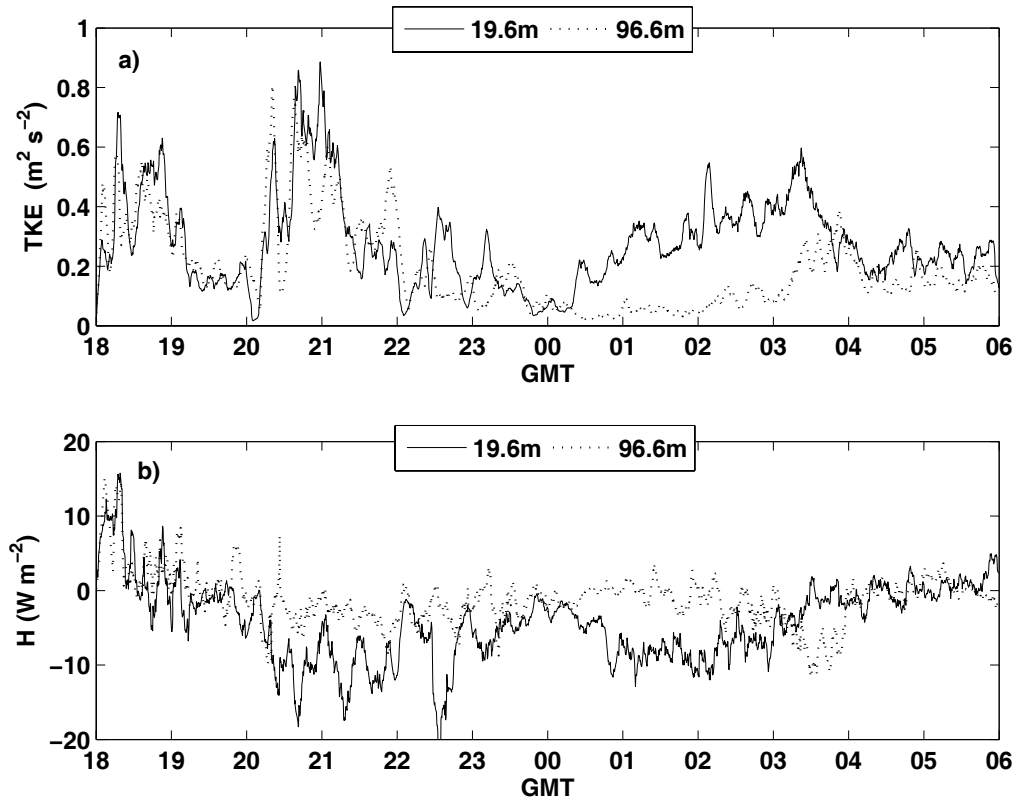
Fig. 13. – a) Turbulent Kinetic Energy and b) vertical heat flux at 19.6 and 96.6 m AGL estimated by means of the wavelet transform.

flux divergence is suppressed, the cooling rate of the air near the ground is considerably slowed down.

From 0000 GMT until the fog onset at 0310 GMT, there is a second increase in the turbulence and decrease in the stability. Nevertheless, unlike in the episode following the katabatic outbreak, the relatively strong turbulence is restricted to the lowest layers, being almost suppressed at the level of 96.6 m AGL (fig. 13a). There is a clearly visible LLJ around 100 m AGL, but the vertical wind shear is not enough to produce a significant amount of TKE. The friction velocity and the vertical heat flux follow a similar pattern, with relatively large values close to ground and very small values aloft. In particular, the vertical heat flux at 96.6 m AGL is very small and its estimates are even temporarily positive.

After the onset of fog, the situation is completely different. The ground inversion disappears and the vertical thermal profile becomes almost neutral. There is a moderate sustained level of turbulence with the TKE slowly decreasing with height. The eddy transfer coefficients are considerably large. Nevertheless, the potential temperature hardly changes with height and, consequently, there is a very small vertical heat flux, positive and restricted to the lowest layers.

5. – Conclusions

This paper presents the analysis of the different regimes of turbulence observed during a single night of the campaign SABLES 2006. Synoptic conditions might lead to predict a relatively calm and stable night, but the actual evolution was driven by the mesoscale circulations established at the whole basin. In a schematic way, the night may be divided concerning turbulence characteristics into three parts, which are respectively moderately stable, weakly stable and neutral. There is a very sudden shift between the different regimes, forced by the outbreak of a katabatic flow and the onset of fog. The presence of waves (with periods greater than 5 minutes) is clearly visible in the pressure records after 2000 GMT and may be well represented by wavelets. When the fog is established the structure of the NBL changes completely: the surface-base inversion disappears, the atmospheric boundary layer is almost neutral with a moderate level of turbulence, and very small heat fluxes are present due to the lack of important thermal stratification.

Both the MRFD and the WT methods have proven to be very useful to analyse the turbulence in the boundary layer. They present important advantages in front of the classical and still widely used method based on the eddy covariance method. In the application of the MRFD method, any previous hypothesis about the time scale of the spectral gap separating turbulence and large-scale motions is stated and the position of this gap is investigated in every case. Nevertheless, the hypothesis of the presence of this gap is not always borne out in the stably stratified boundary layer. The application of the WT method is based on its excellent performance as a filter. The ability of the WT to filter out low-frequency oscillations precludes the need for a spectral gap between high and low frequency oscillations.

The above analysed processes (sudden bursts of turbulence, fog, gravity waves) can be critical to some human activities, such as those related to aeronautics. Nevertheless, the precise evolution of the NBL is rarely captured by the NWP models. A proper understanding of the physical processes occurring at the ABL is very important in order to improve the parameterizations of the turbulent diffusion both in the NWP and in the climate models.

APPENDIX A.

In this appendix the different definitions of the turbulent and stability parameters used in sect. **4** are listed:

– Gradient Richardson Number (Ri_g): This stability parameter comprises information about the dynamic and thermal processes contributing to stability (wind shear

and gradient of potential temperature):

$$(A.1) \qquad Ri_g = \frac{\frac{g}{\theta_0}\frac{\partial\overline{\theta}}{\partial z}}{\left(\frac{\partial\overline{U}}{\partial z}\right)^2 + \overline{U}^2\left(\frac{\partial\overline{\alpha}}{\partial z}\right)^2} \, .$$

To evaluate the gradients of wind velocity and temperature, log-linear fits [32] were made to the different levels data. The wind direction gradient is evaluated using simple linear fits:

$$(A.2) \qquad \begin{aligned} \overline{U} &= az + b\ln z + c, \\ \overline{T} &= a'z + b'\ln z + c', \\ \bar{\alpha} &= a''z + c''. \end{aligned}$$

– The Turbulent Kinetic Energy (TKE), which is the portion of kinetic energy associated with turbulence, evaluated from the variances of the along-wind, cross-wind and vertical components of velocity:

$$(A.3) \qquad TKE = \frac{1}{2}\left(\overline{u'^2} + \overline{v'^2} + \overline{w'^2}\right).$$

– Inversion strength. This stability parameter is defined as the temperature difference between $35.5\,\text{m}$ and $2.3\,\text{m}$.

$$(A.4) \qquad \Delta T_{35.5-2.3} = T_{35.5\,\text{m}} - T_{2.3\,\text{m}}.$$

– The turbulent exchange coefficients of momentum and heat (K_m, K_h), which are the turbulent counterpart to the molecular kinematic viscosity and thermal diffusivity coefficients:

$$(A.5) \qquad K_m = -\frac{\overline{u'w'}}{(\partial\overline{U}/\partial z)},$$

$$(A.6) \qquad K_h = -\frac{\overline{\theta'w'}}{(\partial\overline{\theta}/\partial z)}\,.$$

– Friction velocity, which is related to the vertical shear of the wind speed:

$$(A.7) \qquad u_* = \left[(-\overline{u'w'})^2 + (-\overline{v'w'})^2\right]^{1/4}.$$

– Sensible Heat Flux. This is an important term of the energy balance equation. It usually takes negative values at stable conditions, when the thermal stratification determines a transfer of heat towards the surface:

$$(A.8) \qquad H = \rho c_p \overline{\theta'w'}.$$

REFERENCES

[1] STULL R. B., *An Introduction to Boundary Layer Meteorology* (Kluwer Academic Publishers, Dordrecht) 1988.

[2] CUXART J., YAGÜE C., MORALES G., TERRADELLAS E., ORBE J., CALVO J., FERNÁNDEZ A., SOLER M. R., INFANTE C., BUENESTADO P., ESPINALT A., JOERGENSEN H. E., REES J. M., VILÁ J., REDONDO J. M., CANTALAPIEDRA I. R. and CONANGLA L., *Boundary-Layer Meteorol.*, **96** (2000) 337.

[3] POULOS G. S., BLUMEN W., FRITTS D. C., LUNDQUIST J. K., SUN J., BURNS S. P., NAPPO C., BANTA R., NEWSOM R., CUXART J., TERRADELLAS E., BALSLEY B. and JENSEN M., *Bull. Am. Meteorol. Soc.*, **83** (2002) 555.

[4] YAGÜE C., VIANA S., MAQUEDA G., LAZCANO M. F., MORALES G. and REES J. M., *Física de la Tierra*, **19** (2007) 37.

[5] CONANGLA L., CUXART J. and SOLER M. R., *Boundary-Layer Meteorol.*, **128** (2008) 255.

[6] GRACHEV A. A., FAIRALL CH. W., PERSSON P. O. G., ANDREAS E. L. and GUEST P. S., *Boundary-Layer Meteorol.*, **116** (2005) 201.

[7] YAGÜE C. and REDONDO J. M., *Antarc. Sci.*, **7** (1995) 421.

[8] NAPPO C. J., *An Introduction to Atmospheric Gravity Waves* (Academic Press, San Diego) 2002.

[9] MUSK L. F., Chapt. 6 in *Highway Meteorology*, edited by PERRY A. H. and SYMONS L. J. (E and FN Spon, London) pp. 91-130.

[10] TALLEY W. K., *Appl. Econ.*, **31** (1999) 1365.

[11] ALLAN S. S., GADDY S. G. and EVANS J. E., *Lincoln Laboratory Project Report ATC-291* (Massachusetts Institute of Technology, Lexington, MA) 2001.

[12] BERGOT T., TERRADELLAS E., CUXART J., MIRA A., LIECHTI O., MUELLER M. and NIELSEN N. W., *J. Appl. Meteorol. Climatol.*, **46** (2007) 504.

[13] GULTEPE I., TARDIF R., MICHAELIDES S. C., CERNAK J., BOTT A., BENDIX J., MÜLLER M. D., PAGOWSKI M., HANSEN B., ELLROD G., JACOBS W., TOTH G. and COBER S. G., *Pure Appl. Geophys.*, **164** (2007) 1121.

[14] ROACH W. T., BROWN R., CAUGHEY S. J., GARLAND J. A. and READINGS C. J., *Q. J. R. Meteorol. Soc.*, **102** (1976) 313.

[15] WELCH R. M. and WELICKI B. A., *J. Appl. Meteorol.*, **25** (1986) 101.

[16] ZHOU B. and FERRIER B. S., *J. Appl. Meteorol. Climatol.*, **47** (2008) 1704.

[17] TERRADELLAS E., FERRERES E. and SOLER M. R, *Adv. Sci. Res.*, **2** (2008) 31.

[18] SAN JOSÉ R., CASANOVA J. L., VILORIA R. E. and CASANOVA J., *Atmos. Environ.*, **19** (1985) 1555.

[19] VIANA S., YAGÜE C., MAQUEDA G. and MORALES G., *Fśica de la Tierra*, **19** (2007) 55.

[20] HOWELL J. F. and MAHRT L., *J. Atmos. Sci*, **51** (1994) 2165.

[21] HOWELL J. F. and MAHRT L., *Boundary-Layer Meteorol.*, **83** (1997) 117.

[22] VICKERS D. and MAHRT L., *J. Atm. Ocean Tech.*, **20** (2003) 660.

[23] VORONOVICH V. and KIELY G., *Boundary-Layer Meteorol.*, **122** (2007) 1.

[24] TENNEKES H., *J. Atmos. Sci.*, **33** (1976) 1660.

[25] DAUBECHIES I., *Ten Lectures on Wavelets* (Society for Industrial and Applied Mathematics, Philadelphia) 1992.

[26] FARGE M., *Annu. Rev. Fluid Mech.*, **24** (1992) 395.

[27] TERRADELLAS E., MORALES G., CUXART J. and YAGÜE C., *Dyn. Atmos. Oceans*, **34** (2001) 225.

[28] CUXART J., MORALES G., TERRADELLAS E. and YAGÜE C., *Boundary-Layer Meteorol.*, **105** (2002) 305.

[29] TERRADELLAS E., SOLER M. R., FERRERES E. and BRAVO M., *Boundary-Layer Meteorol.*, **114** (2005) 489.

[30] TORRENCE C. and COMPO G., *Bull. Am. Meteorol. Soc.*, **79** (1998) 1.

[31] UNDÉN P., RONTU L., JARVINEN H., LYNCH P., CALVO J., CATS G., CUXART J., EEROLA K., FORTELIUS C., GARCIA-MOYA J. A., JONES C., LENDERLINK G., MCDONALD A., MCGRATH R., NAVASCUES B., NIELSEN N. W., DEGAARD V., RODRIGUEZ E., RUMMUKAINEN M., RÖÖM R., SATTLER K., SASS B. H., SAVIJARVI H., SCHREUR B. W., SIGG R., THE H. and TIJM A., *HIRLAM-5 Scientific Documentation* (HIRLAM-5 Project, Norrkoping, Sweden) 2002.
[32] NIEUWSTADT F. T. M., *J. Atmos. Sci.*, **41** (1984) 2202.